Reduced Space Optimal Interpolation of Historical Marine Sea Level Pressure: 1854–1992*

ALEXEY KAPLAN, YOCHANAN KUSHNIR, AND MARK A. CANE

Lamont-Doherty Earth Observatory, Columbia University, Palisades, New York

(Manuscript received 20 April 1999, in final form 8 October 1999)

ABSTRACT

Near-global 4° × 4° gridded analysis of marine sea level pressure (SLP) from the Comprehensive Ocean–Atmosphere Data Set for monthly averages from 1854 to 1992 was produced along with its estimated error using a reduced space optimal interpolation method. A novel procedure of covariance adjustment brought the results of the analysis to the consistency with the a priori assumptions on the signal covariance structure. Comparisons with the National Centers for Environmental Prediction–National Center for Atmospheric Research global atmosphere reanalysis, with the National Center for Atmospheric Research historical analysis of the Northern Hemisphere SLP, and with the global historical analysis of the U.K. Meteorological Office show encouraging skill of the present product and identifies noninclusion of the land data as its main limitation. Marine SLP pressure proxies are produced for the land stations used in the definitions of the Southern Oscillation and North Atlantic Oscillation (NAO) indices. Surprisingly, they prove to be competitive in quality with the land station records. Global singular value decomposition analysis of the SLP fields versus sea surface temperature identified three major patterns of their joint large-scale and long-term variability as ''trend,'' Pacific decadal oscillation, and NAO.

1. Introduction

The monthly averaged sea level pressure (SLP) can be viewed as a physical variable that together with sea surface temperature (SST) describes the large-scale behavior of the ocean–atmosphere interface, the medium of crucial dynamical importance for the climate and its variability. For the presatellite era, the main source of observations of this interface are the measurements taken on volunteer observing ships. As a result, the observational coverage reflects ship traffic variations, being incomplete at present, quite sparse before 1950, and virtually nonexistent before the middle of the nineteenth century. Compilations of such observations into binned averages on a regular latitude–longitude grid with quality control and other statistics have become available during the last decade [e.g., Comprehensive Ocean–Atmosphere Data Set (COADS), Woodruff et al. 1987; Global Ocean Surface Temperature Atlas (GOSTA), Bottomley et al. 1990]. We recently developed a method for objective optimal analysis of such historical datasets (Kaplan et al. 1997), and applied it to the MOHSST5 version of GOSTA (Parker et al. 1994), producing near-global analysis of monthly SST anomalies for the period 1856–1991 (Kaplan et al. 1998, hereafter K98). This method combines a classic approach of least squares optimal estimation with the novelty of space reduction and is specifically designed to recover large-scale features of the observed variable. These features are presumed to be of largest climatic importance, and they are essentially all of the robust signal that can be derived from sparse data. Here we apply a similar approach to the COADS compilation of SLP observations.

The goal of this work is to produce an optimal analysis of SLP with estimated uncertainty, based solely on marine observations. Such a product will be useful for the baseline comparison of more elaborated analyses (those making use of land station data, atmospheric models, etc.) that might be produced in the future.

While we were attempting to apply to the COADS SLP data exactly the same technique we used in K98, the differences in the data produced a few alternations in the procedure. To the large extent, these differences are caused by the different nature of estimated variables. SLP is known to have larger scales of spatial coherence than SST has but a much whiter temporal spectrum (Davis 1976). Consequently, the spatial interpolation of SLP data with main patterns of SLP variability that can be approximated by eigenvectors of the data sample covariance matrix [also known as empirical orthogonal

* Lamont-Doherty Earth Observatory Contribution Number 5982.

Corresponding author address: Dr. Alexey Kaplan, Lamont-Doherty Earth Observatory, Columbia University, P.O. Box 1000, 61 Route 9W, Palisades, NY 10964-8000.
E-mail: alexeyk@ldeo.columbia.edu

functions (EOFs)] has good prospects, but temporal smoothing probably will not be useful. As a result, instead of the reduced space optimal smoothing technique of K98, we use reduced space optimal interpolation here.

In section 2 we provide a short description of the procedure, concentrating on the differences between the present application and K98. The rest of the paper deals with the verification of the product we developed. In section 3 it is compared with the National Centers for Environmental Prediction–National Center for Atmospheric Research (NCEP–NCAR) global atmosphere reanalysis (Kalnay et al. 1996), with a historical analysis of the Northern Hemisphere SLP (Trenberth and Paolino 1980), and with the analysis GMSLP2.1f of the U.K. Meteorological Office (Basnett and Parker 1997). In section 4 we use the analysis to estimate the SLP values at locations of a few land stations—Darwin, Tahiti, Reykjavik, and Gibraltar—in order to verify the results and theoretical error estimates against independent data. We also produce and validate the analysis versions of the Souther Oscillation and North Atlantic Oscillation indices. Section 5 presents verification of more subtle features of the analysis, its representation of the long-term variability of SLP and SST, while section 6 discusses results and makes conclusions.

2. Data and their analysis

a. Observational data for the analysis

The SLP data consist of monthly summary trimmed groups (MSTGs) from release 1 of COADS (years 1854–1979; Woodruff et al. 1987) extended by standard release 1a (years 1980–92; Woodruff et al. 1993). MSTG data do not contain individual measurements but instead provide monthly summary statistics of the sets of measurements in $2^\circ \times 2^\circ$ boxes arranged in a regular spatial grid. In addition to COADS regular quality control procedures, the data for MSTG statistics are subjected to the additional ''trimming'' procedure, which identifies and excludes outliers with respect to climatological 3.5σ limits derived from data for periods 1854–1909, 1910–49, and 1950–79, the latter period limits being used also for standard release 1a. Our analysis procedure uses two statistical characteristics of the measurements inside $2^\circ \times 2^\circ$ monthly boxes: mean SLP (p) and the number of observations (n_{obs}). We also use the standard deviations (σ) for the recent (1980–92) period in order to estimate the SLP intrabox variability, which we use for estimating sampling error in the box mean values.

The present version of COADS provides particularly poor SLP data coverage prior to World War II, as compared to, for example, SST data coverage for the same period. According to Woodruff et al. (1998), in ''Dutch'' deck, a major component of COADS data for the period 1854–1938, SLP data is not translated from millimeters to millibars (this requires a correction for gravity) and thus is omitted from the MSTG data.

b. Estimating the annual cycle and monthly anomalies

The analysis is of the monthly anomalies, that is, deviations from the climatological annual cycle. We computed the anomalies with respect to the climatological annual cycle estimated from data collected during the period 1951–80 [the period used by Parker et al. (1994) in estimating anomalies for their MOHSST5 product, which was analyzed by K98]. While averaging monthly values of $2^\circ \times 2^\circ$ boxes for each calendar month over the 30 yr, we weight each monthly value by the number of individual observations available for that box in that month. Such weights minimize the impact of random instrumental and sampling error on resulting averages. After averaging and obtaining a 12-month climatology, we apply a binomial 1–2–1 filter periodically in time, and a fourth-order Shapiro filter (Shapiro 1971) in space. As a result of these steps, we obtain a spatially and temporally smooth climatology that is then subtracted from the COADS values according to the calendar month, in order to obtain $2^\circ \times 2^\circ$ anomalies.

c. Covariance estimation

As emphasized in K98, reliable estimation of the space covariance matrix is the most crucial element of our method. To obtain faithful field reconstructions, we have to use a relatively long time period for the covariance estimation, and there should be enough data in it for estimating all necessary cross covariances. With this in mind, we attempt to estimate covariance for the period 1951–92, which starts with a steep postwar increase in data coverage. As in K98, we define the domain of the analysis by the requirement that the observations are available for more than half of the time points for every spatial box included. The initial attempt to apply this approach to the original COADS $2^\circ \times 2^\circ$ bins produces a very impractical domain: large gaps in the equatorial Pacific are left uncovered, as well as smaller areas in the Indian Ocean and the South Atlantic. Starting in the 1960s instead of the 1950s does not make much difference. In order to improve the spatial coverage of the estimated covariance (and, subsequently, the analyzed data), we have to decrease resolution by uniting COADS $2^\circ \times 2^\circ$ boxes into larger bins. This procedure is justified by the fact that the SLP anomalies usually have larger spatial scales than the climatology. While the switch to 2° latitude $\times$ 4° longitude bins still leave many ''holes,'' averaging data into $4^\circ \times 4^\circ$ boxes basically solves the problem. This example demonstrates the restriction that existing marine observational coverage imposes on the spatial resolution of the covariance estimate based on (at least) a few decades, and

thus it sets the limit on the possible resolution of the historical climate analyses based solely on the observed covariance, without any additional special assumptions of its small-scale behavior.

After averaging $2° \times 2°$ box means into those of $4° \times 4°$ boxes (weighting every value by the number of observations that was used to obtain it), we estimate a space $\times$ space sample covariance matrix and subject it to the procedures of K98 intended to suppress the influence of observational and sampling error: we apply a fourth-order Shapiro filter to rows and columns of the sample covariance matrix, then test the variance decrease against our estimate of data error [diagonal of matrix $\mathbf{R}$ in Eq. (4) below]. If the decrease is larger than the error estimate, we inflate the variance accordingly while preserving correlation structures of the filtered covariance. Unlike K98, in the present application the heuristic procedure of redistributing the variance among eigenvalues [see Eq. (19) in Kaplan et al. (1997)] did not give proper consistency with the distribution of energy over EOF modes in the analyzed solution. Because of that we had to develop a more complicated procedure, which is described in the appendix. This new procedure allows us to achieve consistency between the expected and actual covariances of the analyzed solution and to add reliability to its theoretical error estimates.

d. Space reduction

We present the resulting covariance matrix $\mathbf{C}$ in its canonical form:

$$\mathbf{C} = \mathbf{E}\mathbf{\Lambda}\mathbf{E}^{\mathrm{T}} + \mathbf{E}'\mathbf{\Lambda}'\mathbf{E}'^{\mathrm{T}}. \quad (1)$$

Here $\mathbf{\Lambda}$ is the diagonal matrix that contains the L largest eigenvalues (the reduced phase space); the remainder of the spectrum, $\mathbf{\Lambda}'$, corresponds to the modes dominated by noise and error. Further, $\mathbf{E}$ and $\mathbf{E}'$ are matrices whose columns are eigenvectors (EOFs) corresponding to the eigenvalues contained in $\mathbf{\Lambda}$ and $\mathbf{\Lambda}'$, respectively. The leading L eigenvectors define the reduced space of the main modes of large-scale variability in which we will be looking for an analyzed solution. The discarded part of the total space is too contaminated by noise to yield any structured information. For each month we approximate the SLP field $\mathbf{T}$ by its projection on the L-dimensional space of leading eigenvectors,

$$\mathbf{T} = \mathbf{E}\boldsymbol{\alpha}, \quad (2)$$

and looking for the optimal estimate of the L-dimensional vector of coefficients $\boldsymbol{\alpha}$.

In K98 we compared with partially independent data the analyses of SST with widely varying L and chose $L = 80$ to be the best. At the same time we noticed that the results of the analysis are affected only slightly by changes in L within 50%. Similar to SST resolution at the worse coverage and higher random error of SLP data suggest not to use more than 80 EOFs for the SLP analysis. Because of that we run the analysis with $L = 80$ retaining almost 70% of the total variance.

e. Cost function

For each time point (month) in the record the reduced space optimal interpolation (OI) solution for α minimizes the cost function

$$S[\boldsymbol{\alpha}] = (\mathbf{H}\mathbf{E}\boldsymbol{\alpha} - \mathbf{T}^o)^{\mathrm{T}}\mathbf{R}^{-1}(\mathbf{H}\mathbf{E}\boldsymbol{\alpha} - \mathbf{T}^o) + \boldsymbol{\alpha}^{\mathrm{T}}\mathbf{\Lambda}^{-1}\boldsymbol{\alpha}, \quad (3)$$

where $\mathbf{T}^o$ is a vector of available SLP observations, $\mathbf{H}$ is a transfer operator from the full grid representation of the SLP field $\mathbf{T}$ to the available observations

$$\mathbf{T}^o = \mathbf{H}\mathbf{T} + \boldsymbol{\varepsilon}^o,$$

and $\mathcal{R} = \langle \boldsymbol{\varepsilon}^o \boldsymbol{\varepsilon}^{o\mathrm{T}} \rangle$ is the covariance of sum of observational error (which includes both instrumental and sampling types of error) and representational error [which is an error of approximation (2)]. Since observations are averaged into $4° \times 4°$ boxes, both $\mathbf{T}$ and $\mathbf{T}^o$ are on the same grid so that $\mathbf{H}$ is just a ''sampling'' operator (a submatrix of the identity matrix that includes only rows corresponding to available observations).

The error covariance

$$\mathcal{R} = \mathbf{R} + \mathbf{H}\mathbf{E}'\mathbf{\Lambda}'\mathbf{E}'^{\mathrm{T}}\mathbf{H}^{\mathrm{T}} \quad (4)$$

consists of two terms. The usual data error covariance, $\mathbf{R}$, accounts for the instrumental and sampling error in $4° \times 4°$ box monthly means. It is represented by a diagonal matrix with the elements $\langle \sigma^2_{4\times4} \rangle / N_{\mathrm{obs}}$ on diagonal, where N_{obs} is number of observations contributing to the $4° \times 4°$ box statistics, and $\langle \sigma^2_{4\times4} \rangle$ is intrabox measurement variability estimated through averaging over a recent well-sampled period (1983–92). The idea behind this estimate is that the error in the monthly averaged box value is related to the high-frequency, submonthly variability (due to sampling variability and observational errors) typical to that box (Leith 1973; Trenberth et al. 1992). The $4° \times 4°$ intrabox variances are estimated from the individual statistics for $2° \times 2°$ subboxes included in COADS (mean p, standard deviation σ, and number of observations n_{obs}) using

$$\sigma^2_{4\times4} = \sum_{i=1,\ldots,4} \frac{n_{\mathrm{obs}\ i}(\sigma_i^2 + p_i^2)}{N_{\mathrm{obs}}} - \left(\sum_{i=1,\ldots,4} \frac{n_{\mathrm{obs}\ i} p_i}{N_{\mathrm{obs}}} \right)^2,$$

$$N_{\mathrm{obs}} = \sum_{i=1,\ldots,4} n_{\mathrm{obs}\ i}.$$

The square root of average values of $\langle \sigma^2_{4\times4} \rangle / N_{\mathrm{obs}}$ for the period 1951–92 is shown in Fig. 1a. The second term in $\mathcal{R}$ accounts for the covariance created in the truncated modes $\mathbf{E}'$, the covariance not resolved by the analysis (Fig. 1b).

f. Analyzed solution

Because of the first term in the formulation of the cost function (3), the minimization of S will constrain

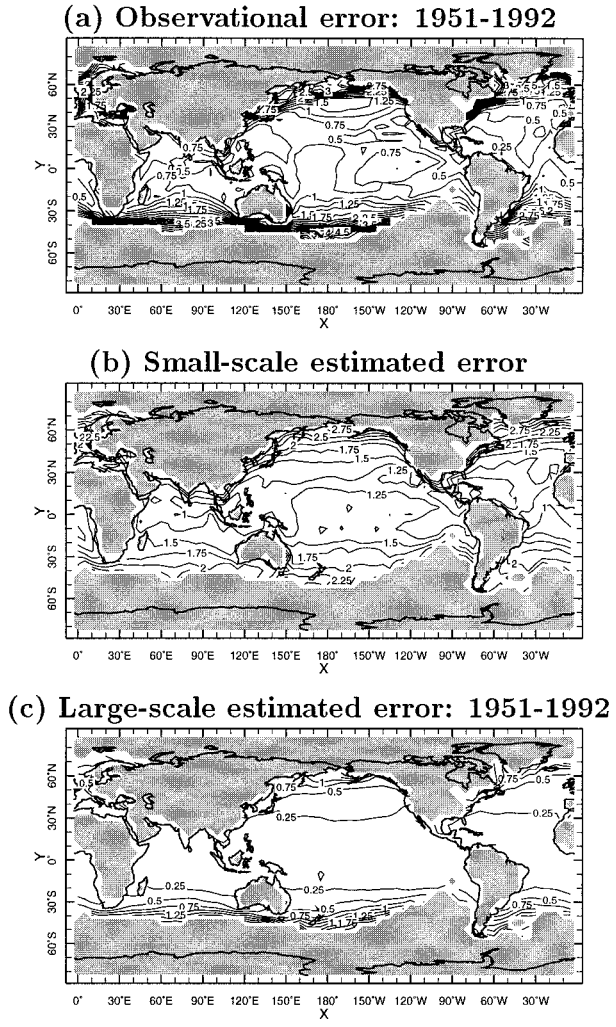

FIG. 1. The rms error estimates in millibars: (a) observational error of 4° × 4° box means for 1951–92, (b) error due to the truncation: the variance in the EOFs beyond $L = 80$, and (c) large-scale estimated error: 1951–92.

the solution to be close to the observed data (within the uncertainty defined by observational error). The second term confines the distribution of energy over the modes of variability to that found in the data (i.e., a derived temporal coefficient of a given eigenvector cannot have more variance than the corresponding eigenvalue). In contrast with the SST analysis presented in K98, the small month-to-month persistence in the SLP field even for the leading modes of variability did not allow us to incorporate a model of time transitions into the analysis and implement the optimal smoother. Here we have to stop at the level of optimal interpolation.

Minimizing S gives the OI solution

$$\hat{\boldsymbol{\alpha}} = \mathcal{P}\mathbf{E}^{\mathrm{T}}\mathbf{H}^{\mathrm{T}}\mathcal{R}^{-1}\mathbf{T}^{o},$$

where

$$\mathcal{P} = (\mathbf{E}^{\mathrm{T}}\mathbf{H}^{\mathrm{T}}\mathcal{R}^{-1}\mathbf{H}\mathbf{E} + \boldsymbol{\Lambda}^{-1})^{-1}$$

is a theoretical estimate for error covariance in the solution.

This reduced space OI solution can be converted into its full grid representation by

$$\hat{\mathbf{T}} = \mathbf{E}\hat{\boldsymbol{\alpha}}; \qquad \mathbf{P} = \mathbf{E}\mathcal{P}\mathbf{E}^{\mathrm{T}}.$$

It should be kept in mind that despite being presented in the full grid space, $\mathbf{P}$ only accounts for the large-scale error (its rms for 1951–92 is shown in Fig. 1c). Here $\mathbf{T}$ does not have any variability corresponding to the modes with numbers higher than L. These modes contribute to an additional error against unfiltered reality with covariance

$$\mathbf{P}^{r} = \mathbf{E}'\boldsymbol{\Lambda}'\mathbf{E}'^{\mathrm{T}}$$

(cf. the second term in the formula for $\mathbf{R}$ above). The standard deviation of this error is shown in Fig. 1b.

3. Analysis verification

Here we present the systematic comparison of our OI analysis of COADS SLP with four other products: raw COADS data (averaged into 4° boxes, as described above), SLP from the Climate Data Assimilation System (CDAS) reanalysis project run jointly by NCEP and NCAR (Kalnay et al. 1996), Trenberth and Paolino (1980) Northern Hemisphere SLP analysis (hereafter NCAR NH analysis), and the recent GMSLP2.1f analysis produced in the Hadley Centre of the U.K. Met. Office by Basnett and Parker (1997) (hereafter the UKMO analysis), which supercedes its earlier version presented by Allan et al. (1996). The CDAS reanalysis is the output of a state-of-the-art atmospheric numerical weather prediction model (albeit with reduced resolution) with a sophisticated three-dimensional spectral variational scheme of data assimilation through which a great deal of observed data (global rawisonde data, surface marine data, aircraft data, surface land synoptic data, satellite sounder data, Special Sensor Microwave/Imager surface wind speeds, satellite cloud drift winds, etc.) is being reconciled with the model dynamics. We take the CDAS reanalysis SLP output to be the reference standard against which all other products are verified.

The NCAR NH analysis, available on monthly 5° × 5° grids starting in 1899, is a compilation of historical weather charts for different regions. U.S. Navy operational analyses are used from July 1962. An elaborate procedure was used to identify, and where possible correct, suspicious data. The UKMO analysis is based on median blending of a few previously existing gridded analyses of historical SLP (NCAR NH included) with marine and land observations, and involves a sophisticated sequence of corrections and smoothing. Therefore, it should come as no surprise that there is a certain degree of similarity between all three of these analyses (CDAS, NCAR NH, and UKMO). All three analyses use the land station data and benefit from the general principles of operational meteorological analysis, albeit

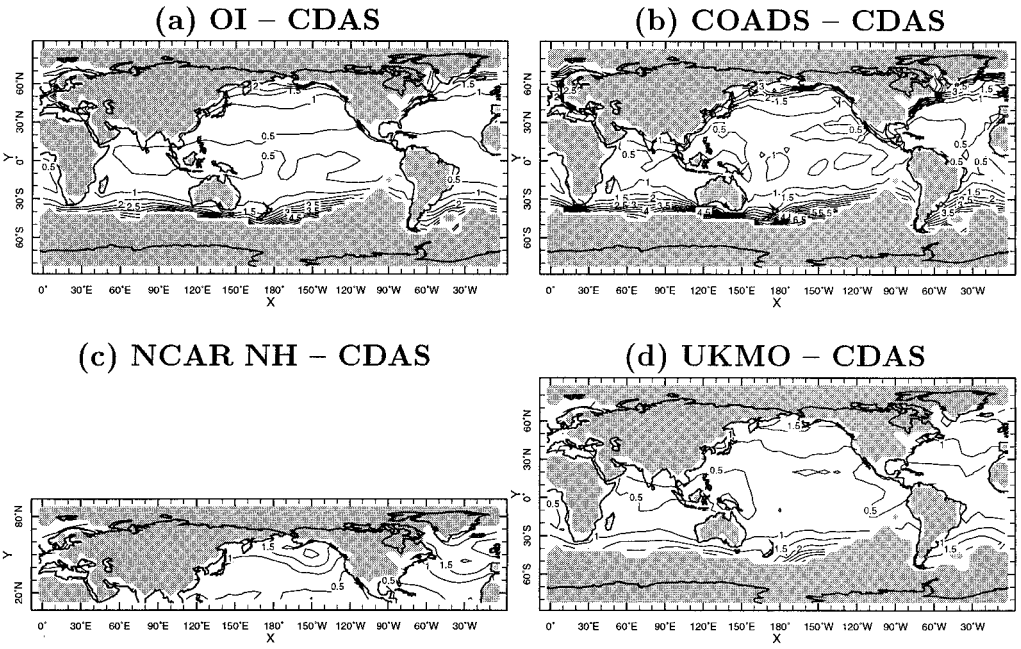

FIG. 2. The rms differences (mb) for 1958–92 between CDAS reanalysis SLP and (a) OI, (b) COADS, (c) NCAR NH, and (d) UKMO SLP products.

implemented differently in different products. In contrast, our product uses nothing but raw COADS marine observations and the generic principles of reduced space optimal estimation.

The comparison is done for three intervals of time: the most recent one, 1958–92, for which all products are available; the intermediate period 1899–57, for which there are no NCEP–NCAR model reanalysis but all historical SLP products are available; and the early period 1871–98, for which only UKMO, COADS, and our analysis are available. We also look into equatorial Pacific SLP values for the latter three products at the full length of their common coverage (1871–1992). Before doing comparisons, fields from all products were regridded on the common $5° \times 5°$ grid, and their climatological means for periods of comparison were removed.

a. 1958–92

Spatial patterns of standard deviation of anomalies for all products (not shown) have a great deal of similarity. However, raw COADS has a significant amount of excessive variance compared to CDAS, about $(2 \text{ mb})^2$ on average, which should be interpreted as the variance of the observational and sampling error. The NCAR NH product also shows greater variance, while our OI and the UKMO products are close to CDAS. Both the NCAR NH and UKMO products are clearly superior to ours near coastlines (former analyses use land observations while we do not) and at the southern boundary of our analysis domain. In the ''open ocean,'' however, the OI results seem to be somewhat smoother and more similar to CDAS.

The same tendencies stand out also when the products are compared to CDAS in terms of rms differences (Fig. 2) and correlation coefficients (not shown). The large increase in rms differences with CDAS near continent coastlines and the southern edge of the analysis domain discerned in the raw COADS data is only slightly decreased in the OI analysis, while in both the UKMO analysis and the NCAR NH the use of land observations and operational weather analyses reduce differences with the CDAS in these places.

Comparison of Figs. 2a and 1b shows that our estimate of the truncation error exceeds almost everywhere the OI difference from CDAS. While the latter is expected to be smaller than the total error in the OI analysis (because both products use essentially the same dataset of historical marine SLP observations and because CDAS is probably providing a somewhat smoother version of the reality), the magnitude of the discrepancy suggests that our covariance adjustment procedure (see appendix) overestimated the variance in the tail of the spectrum.

b. 1899–1957

In the Tropics the OI is closer to the UKMO product than to the raw COADS (Fig. 3). In the North Atlantic the UKMO and the NCAR NH analyses are remarkably close (recall that the NCAR NH was used in the UKMO analysis as one of the input sources) and our OI is closer to both of them than to the raw COADS. In the North

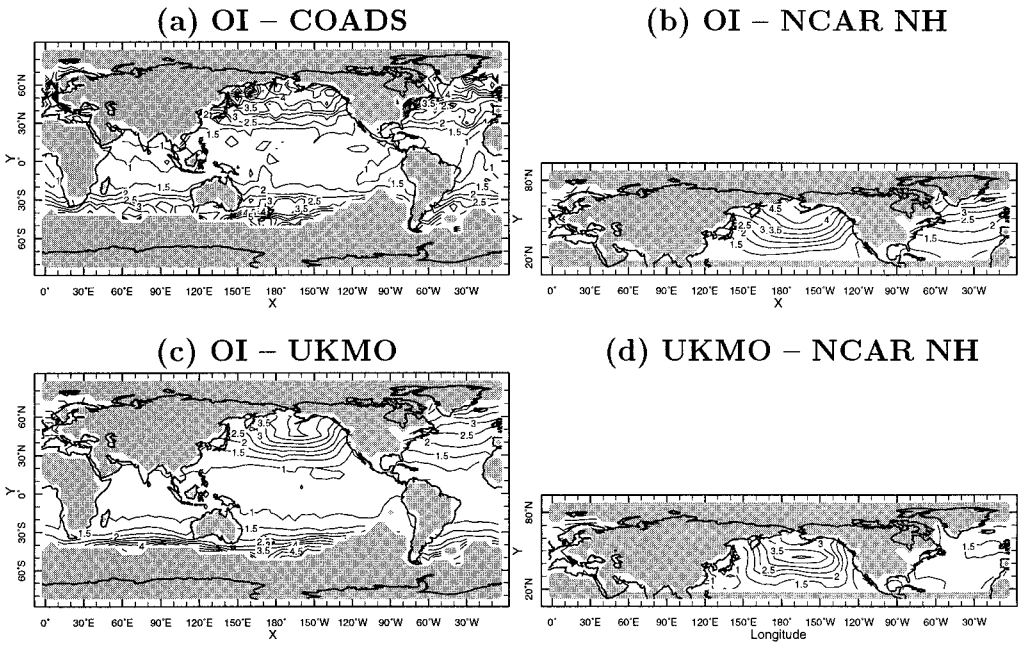

FIG. 3. The rms differences (mb) for 1899–1957 between (a) OI and COADS, (b) OI and NCAR NH, (c) OI and UKMO, and (d) UKMO and NCAR NH.

Pacific, however, the UKMO and NCAR NH have larger differences, and the OI is closer to the UKMO than to the NCAR NH analysis.

For this as well as for the later period the correlation between different products has flat patterns (not shown) of high values in the most of North Pacific and North Atlantic, which decrease steeply toward continental coastlines. Because of that, the rms patterns of Figs. 2 and 3 in these areas resemble scaled-down patterns of standard deviation of SLP anomaly.

c. 1871–98

For this early period of erratic COADS data our OI analysis differs by less than 1 mb rms from the UKMO product in the Tropics and is closer to the UKMO analysis than to the raw COADS everywhere (Fig. 4). In fact, everywhere except for the North Atlantic and the vicinity of the New Zealand, the OI–UKMO difference is smaller for this period than for the period 1899–1957 (cf. Figs. 4b and 3c), because under the condition of extreme data sparsity both analyses exhibit substantially less variance during the former period than during the latter. The UKMO product shows particularly dramatic reduction in the variance of the analyzed anomalies: aside from the North Atlantic and New Zealand, the standard deviation of their marine SLP anomalies rarely exceeds 1 mb, the anomalies being equal to zero for decades in some areas of North Pacific and Southern Hemisphere. Because of this and being based exclusively on the COADS data, the OI is also slightly closer to them than the UKMO product is.

It should be kept in mind that the reliability of the analyzed SLP fields is very low for this period. The variance of the large-scale error alone is comparable to the variance of reconstructed fields themselves in tropics and North Atlantic and exceeds it in the North Pacific and Southern Ocean.

d. Equatorial Pacific

Figure 5 shows aspects of raw COADS data, the UKMO product, our OI, and SST analysis of K98 in the annual mean anomalies for the equatorial Pacific. The OI and UKMO analyses are particularly close to each other for the period 1960–80 and reasonably close for the entire postwar period. For the most of the record the OI analysis produces an expected picture of zonally coherent equatorial variability that mirrors variability in the SST values. In contrast, before 1930 when the COADS data in the area are scarce, the UKMO analysis exhibits a few patches of positive and negative anomalies seemingly dictated by the available island station data. In this case the blending and smoothing technique employed for the UKMO analysis could not effectively smooth out mean discrepancies between different stations resulting in this patchy structure. The obvious shortcoming of our product is the reduction in the variance of the equatorial Pacific during the periods when COADS data are sparse (1910–20 and pre-1870).

4. Sea level pressure indices

Here we use the OI analysis of marine SLP data in order to estimate SLP variations at locations of four

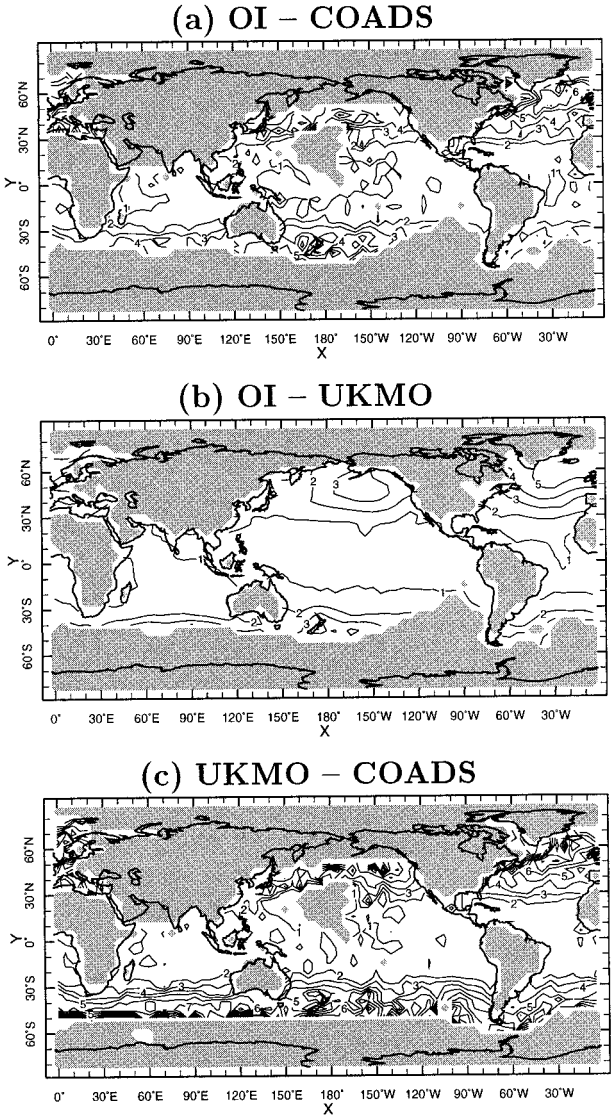

FIG. 4. The rms differences (mb) for 1871–99 between (a) OI and COADS, (b) OI and UKMO, and (c) UKMO and COADS.

land stations where particularly long barometric records are available (Table 1). The SLP records of these stations define widely used climatic indices of North Atlantic Oscillation (NAO) (Jones et al. 1997) and Southern Oscillation index (SOI) (Ropelewski and Jones 1987). We produce marine-based proxies for a land station SLP by averaging the OI analysis values over a few highly correlated $4^\circ \times 4^\circ$ grid boxes surrounding the station, as indicated in Table 1. Such definitions of proxies allow one to use the formalism of Kaplan et al. (1997) to get optimal estimates of the proxies with error bars on them. Large (by far exceeding error bars) differences between station data and proxies can occur in one of a few cases: when land station barometric measurements are in serious error, when surrounding ship data are subject to systematic error, and when SLP on a land station has a large contribution of essentially local effects that cannot be captured by averaging marine SLP over the area of a few grid boxes. Since the land station record consists of monthly averages of many measurements taken at the same location by the same instrument, one expects it to be of superior quality compared to averages of ship measurements over individual grid boxes. Surprisingly, however, the proxies based on the latter prove to be comparable in quality with land station data, except for the periods when marine data coverage is particularly bad.

Table 2 compares monthly time series of Darwin and Tahiti SLP observations with their marine-based proxies. In the recent (1951–92) period of relatively reliable data, both land station records are equally highly correlated with the proxies and show rms deviations from them that are well below theoretical error estimates. Imperfections in the correspondence between stations and proxy values in this period come mostly from high (and incoherent between the two types of records) month-to-month SLP variability. When the latter is filtered by a 5-month running mean filter, the match improves considerably (Figs. 6 and 7). For the earlier periods the correspondence between the station data and proxies worsens, more so for Tahiti (where the deviation exceeds expected error) than for Darwin records. Improvement of proxies on straight averages of local raw marine data is remarkable (Fig. 6). In fact, the truthful reconstructions are not even limited by the availability of the local data, using large-scale correlations with remote data in order to estimate the SLP in the vicinity of the station.

Since Darwin and Tahiti stations are known to capture the variability of the Southern Oscillation, we expect significant anticorrelation of the SLP records at these stations, as well as significant absolute values of the correlation with Niño-3 (mean SST for the eastern equatorial Pacific 5°S–5°N, 150°–90°W; we use optimal estimates of this index from K98). We expect the absolute values of the correlation coefficients to be high for the recent time periods and reduced for the earlier periods of lower quality data. Indeed, as we move from the present to the past the absolute values of the correlation coefficients of station records with Niño-3 decreases: only slightly for Darwin and more appreciably for Tahiti. Note that the marine-based proxy for Tahiti SLP is more robust in terms of its Niño-3 correlation than the station record. Similarly, the two proxies are more strongly anticorrelated with each other than the two station records.

In the spirit of Trenberth (1984), higher correlations between reconstructed indices compared to the land-based ones are interpreted as higher signal-to-noise ratio (in this case ''signal'' is large-scale ENSO-associated phenomena, ''noise'' is everything else). This improvement might take place for two reasons. First, a marine-based proxy might be free from systematic errors in the land station data, which, when they occur, are very dif-

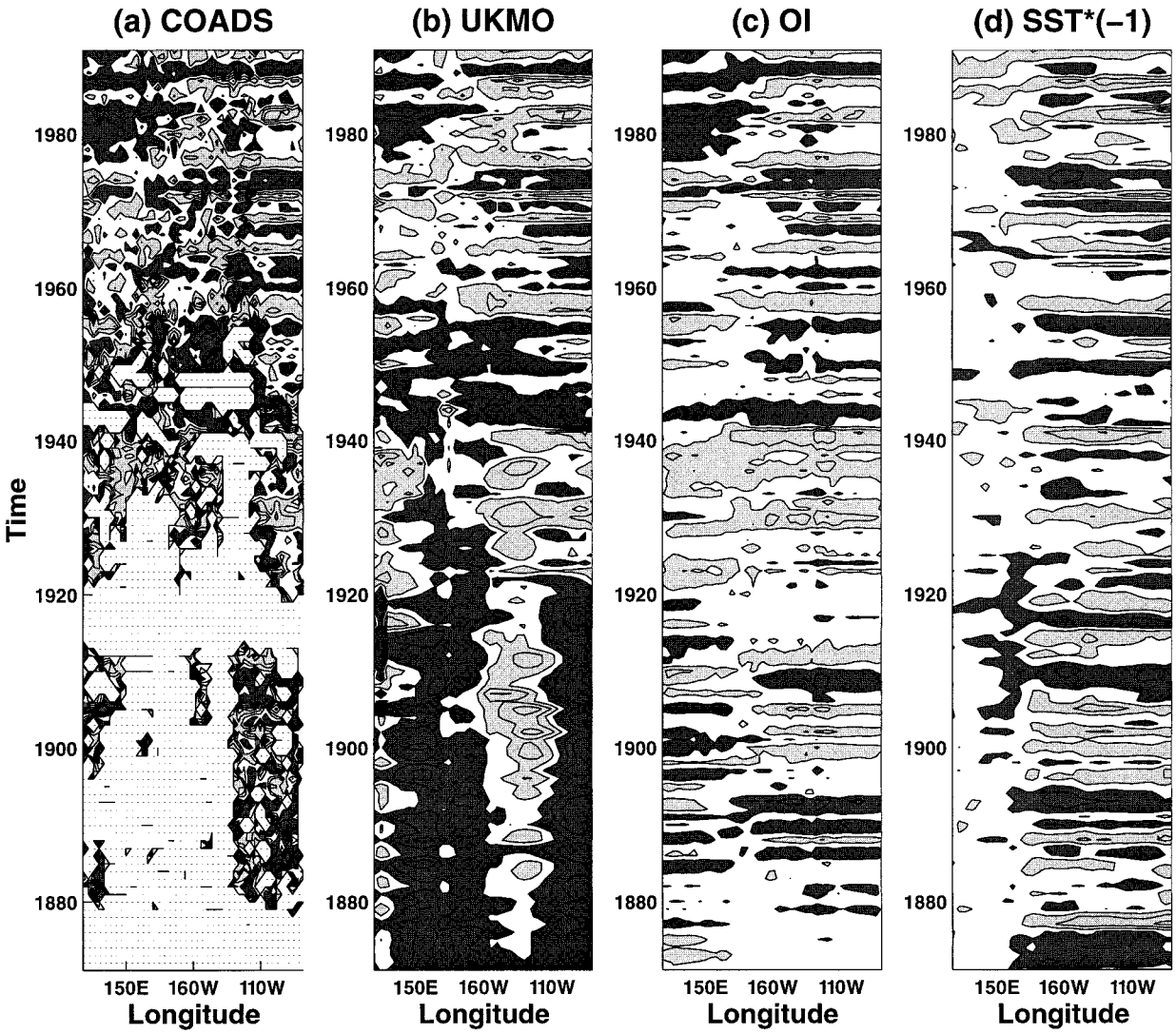

FIG. 5. Equatorial anomalies of (a) COADS SLP (mb), (b) UKMO (mb), (c) OI (mb), and (d) K98 SST anomaly (°C) multiplied by −1. Contour interval for SLP (SST) is 0.5 mb (0.6°C); values higher than 0.25 mb (0.3°C) are shaded dark, lower than −0.25 mb (−0.3°C) are shaded light. Missing data in (a) are dotted.

ficult to correct. For example, there are known to be problems with the Tahiti barometer before 1935 (Ropelewski and Jones 1987; Trenberth and Hoar 1996). Certain biases have been corrected by Ropelewski and Jones (1987) (see their Table 2). Still, the station record shows an almost constant positive anomaly from 1928 to 1932 that does not have a counterpart in either Darwin record, Niño-3 reconstruction, or marine data abundant in the vicinity of Tahiti at that time, leading to the conclusion that Tahiti station data are in error during the period. Also suspicious are the largest in this century positive anomaly in 1917 (incidentally, a year when the barometer was changed; a bias correction of 2 mb was applied to the entire period 1917–25) and uncorrelated

TABLE 1. Land stations and their marine proxies.

Station	Source of the land data	Time period in the source	Marine SLP proxy defined as the OI analysis average over the area
Darwin	Können et al. (1998)	1866–1997	14°–10°S, 128°–132°E
Tahiti	Können et al. (1998)	1855–1997	22°–14°S, 156°–144°W
Gibraltar	Jones et al. (1997)	1821–1997	34°–38°N, 8°W–4°E
Reykjavik	Jones et al. (1997)	1821–1997	62°–66°N, 28°–20°W

TABLE 2. Comparison of land station data with marine-based proxies at Darwin and Tahiti.

Statistics	1855–1900		1901–50		1951–92	
	Darwin	Tahiti	Darwin	Tahiti	Darwin	Tahiti
Correlation between station and proxy	0.45	0.26	0.60	0.31	0.83	0.83
Rms diff between station and proxy (mb)	1.1	1.3	0.84	1.16	0.60	0.56
Rms proxy theoretical error (mb)	1.3	1.1	1.3	0.98	1.2	0.89
Correlation between proxy and Niño-3	0.48	−0.41	0.44	−0.53	0.61	−0.55
Correlation between station and Niño-3	0.51	−0.27	0.56	−0.26	0.61	−0.47
Correlation between proxies	−0.55		−0.36		−0.49	
Correlation between stations	−0.17		−0.25		−0.35	

with other sources variability between 1902 and 1904. Recently recovered early Tahiti data along with regression of the data from other stations were used by Können et al. (1998) to extend the Tahitian record back to 1855 and fill the gaps in it. Figure 7 shows that on both of the most prominent occasions of disagreement between Können et al. (1998) and Ropelewski and Jones (1987) Tahiti records (1905 and 1926), the former is closer to Niño-3 and our OI estimate.

Another reason for the increase in signal-to-noise ratio in the proxy indices is that our technique reconstructs large-scale patterns of variability, and in the periods of poor data coverage it reflects the large-scale Southern Oscillation variability rather than local variability. This explains the fact that the strongest anticorrelation between proxies (−0.55) is achieved in the earliest period, when the data coverage is particularly poor.

The obvious problem with the marine-based proxies is when data availability over the entire global ocean is poor, the optimal estimate will tend to produce no var-

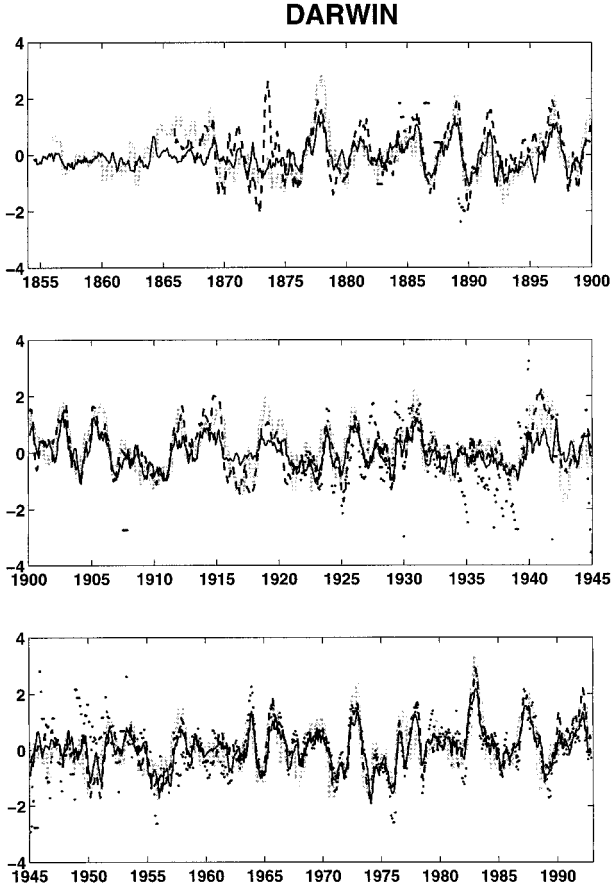

FIG. 6. Five-month running mean SLP anomaly (mb) at Darwin: land station record (dashed line), OI proxy (solid line), and raw COADS proxylike average (dots). Niño-3 (°C) is shown by a thick light line.

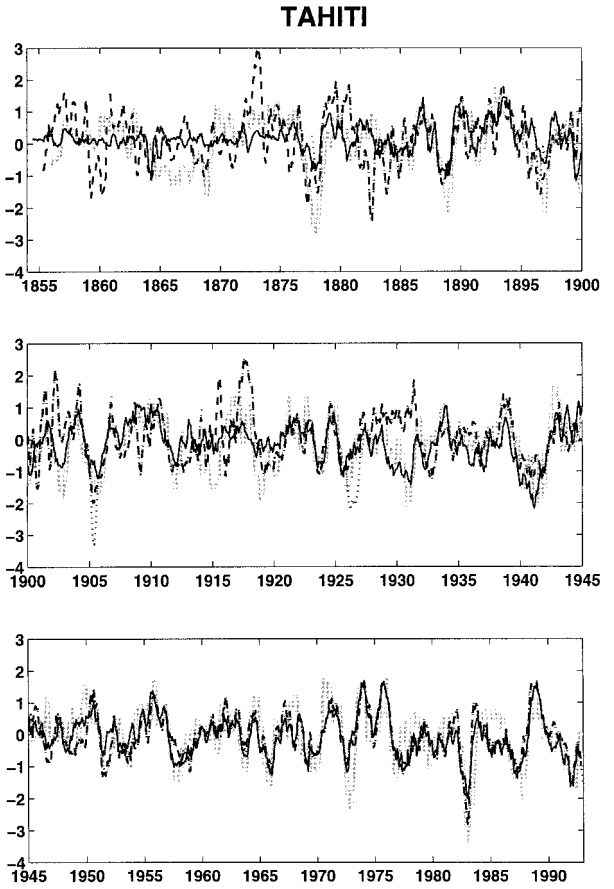

FIG. 7. Five-month running mean SLP anomaly (mb) at Tahiti: land station records compiled by Können et al. (1998) (dashed line) and Ropelewski and Jones (1987) (dots), and OI proxy (solid line). Niño-3 (°C) multiplied by −1 is shown by a thick light line.

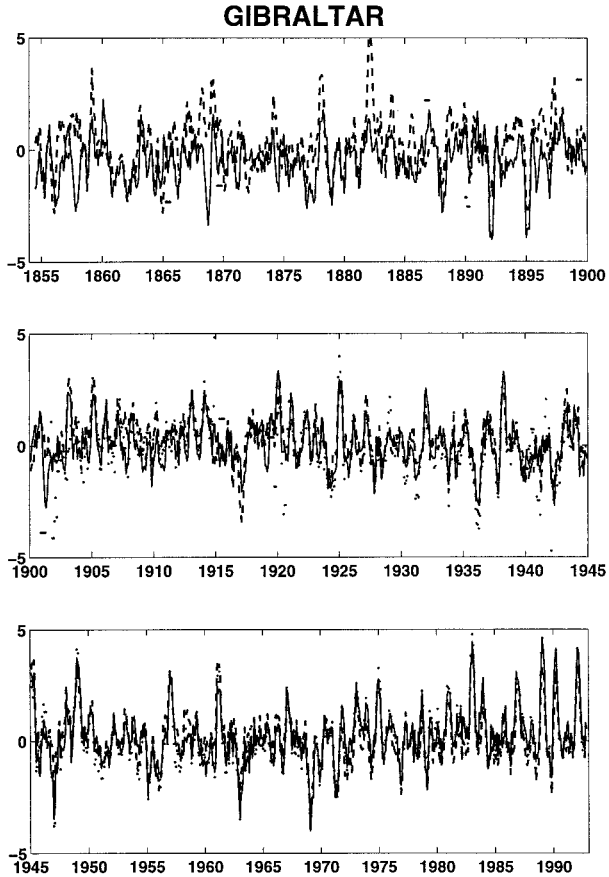

FIG. 8. Five-month running mean SLP anomaly (mb) at Gibraltar: land station record (dashed line), OI proxy (solid line), and raw COADS proxylike average (dots).

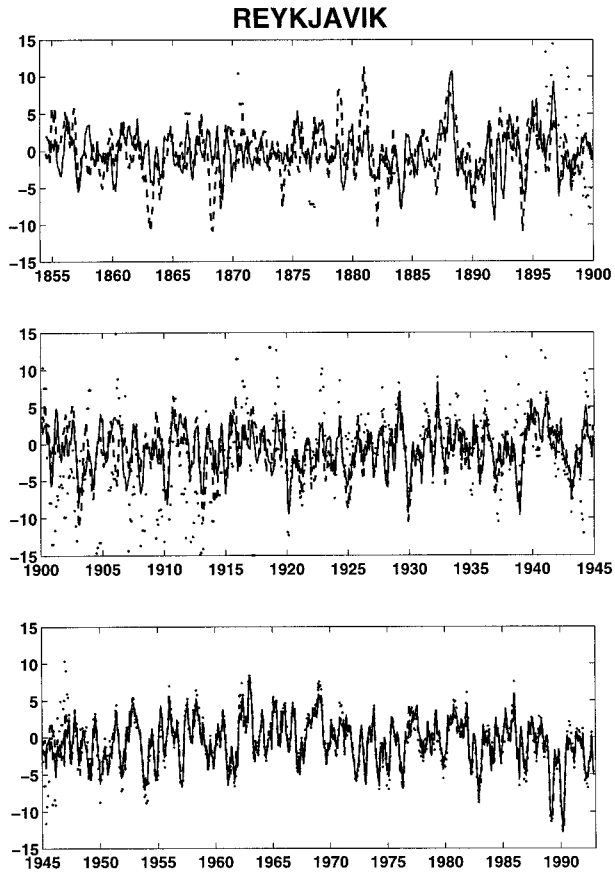

FIG. 9. Five-month running mean SLP anomaly (mb) at Reykjavik: land station record (dashed line), OI proxy (solid line), and raw COADS proxylike average (dots).

iability, as is the case with the Darwin and Tahiti reconstructions before 1875 (Figs. 6 and 7). This seems to be less the case for Gibraltar and Reykjavik SLP marine-based proxies, which take advantage of good North Atlantic data coverage (Figs. 8 and 9). Otherwise the tendencies in the Atlantic proxy correlations are consistent with what was observed for tropical stations (Figs. 8 and 9, and Table 3).

Figure 10 compares SOI and NAO indices based on the proxies (seasonal and winter values respectively) with those based on land station data. The match seems almost perfect in the recent decades and degraded during earlier times. This suggests that mismatches are mainly due to the decreased data quality rather than to the difference in the definition of marine-based and land-based indices. We show monthly values of Niño-3 on SOI panel as well. Two of the most prominent occasions when land-based SOI differs from the two other curves (around 1917 and 1930) are traceable to problems in the Tahiti station record.

5. Global climate variability in the SLP analysis

Using the SLP analysis described above, and the SST analysis of K98, we seek to identify the leading patterns of global climate variability during the last century or

TABLE 3. Comparison of land station data with marine-based proxies at Gibraltar and Reykjavik.

Statistics	1855–1900		1901–50		1951–92	
	Gibr	Reyk	Gibr	Reyk	Gibr	Reyk
Correlation between station and proxy	0.52	0.48	0.81	0.79	0.92	0.97
Rms diff between station and proxy (mb)	2.3	6.3	1.4	4.2	0.98	1.7
Rms proxy theoretical error (mb)	2.0	5.2	1.4	3.0	1.2	2.1
Correlation between proxies	−0.57		−0.48		−0.49	
Correlation between stations	−0.48		−0.49		−0.47	

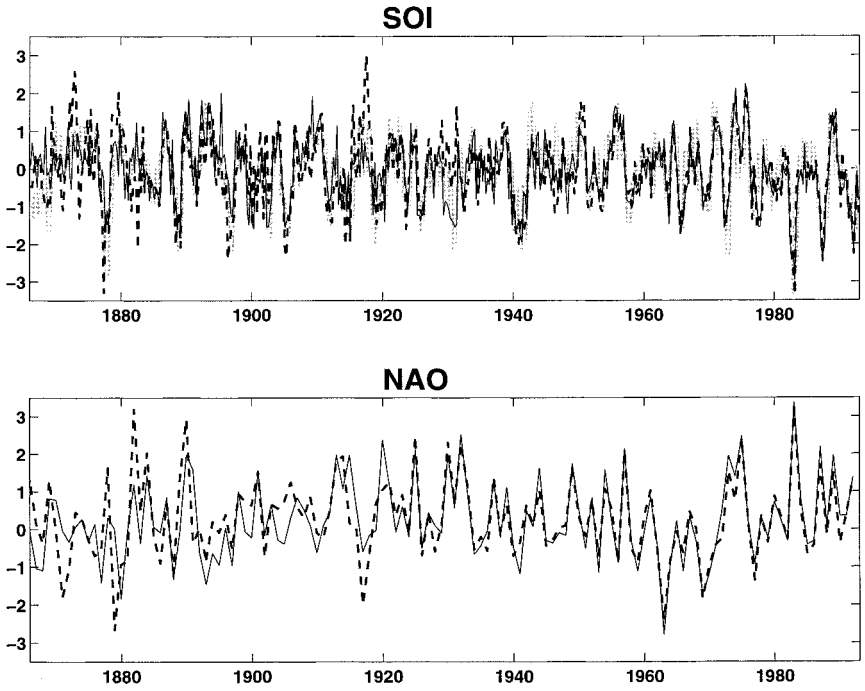

FIG. 10. Comparison of land-based (dashed lines) and marine-based (solid lines) oscillation indices. Seasonal means for SOI and winter means for NAO are shown. SOI panel shows also Niño-3 multiplied by −1 in a thick light line.

so. We apply a running 5-yr means filter to annual averages of the 80 time coefficients corresponding to SLP and SST, respectively (the direct results of the reduced-space analysis procedure), and calculate the covariance matrix between the two fields. We then perform a singular value decomposition (SVD) analysis of this 80 × 80 covariance matrix to determine the linear combinations of each set of coefficients (SLP and SST) that would lead to time series that maximize the covariance between the two fields. We then regress the full data on these time series to uncover the spatial patterns of each field corresponding to these modes. The procedure is equivalent to that described by Bretherton et al. (1992) and can be thought of as the latter's reduced space version. The leading three heterogeneous patterns (the regression of each field on the normalized time series of the other) are shown in Fig. 11, and the time series are in Fig. 12.

The dominant pattern of SLP–SST covariability explains 29% of the covariance, and the correlation between the two corresponding time series is 0.73. Together, the SST time series and pattern (Fig. 12, top panel, and Fig. 11, top left panel) describe a century-long warming of the world ocean. The SST time series is quite similar to that of globally averaged SST (e.g., Nicholls et al. 1996; their Fig. 3.3). The warming is not uniform in either space or time. During the last 90 years or so, there are two intervals of conspicuous warming, one between 1920 and 1950, and the other after 1975 or so.

The pattern is quite similar to the one described in Cane et al. (1997). It indicates that most ocean areas contribute positively to the warming trend, with the strongest warming occurring in the Southern Hemisphere. However, some oceanic regions display a non-committal cooling trend. These regions are found in the tropical Pacific, North Pacific, and North Atlantic Oceans. Cane et al. (1997) interpret this patterns, in particular the equatorial Pacific cooling, as the response of the regional equatorial atmosphere–ocean system to global warming induced by the increase in CO_2. However, the robustness of the equatorial signature has been questioned by others (e.g., Hurrell and Trenberth 1999). The regions where the SST changes are most significant (as judged by the heterogeneous correlation patterns, not shown) are in the South Atlantic and Indian Oceans, and in the western tropical and South Pacific Ocean, west of the date line. Overall the pattern explains 11% of the analysis area SST variance.

The corresponding leading SLP time series (Fig. 12, top panel) indicates a negative trend in the last few decades of the nineteenth century and positive trend in the twentieth century. The trend is disrupted by a sharp fluctuation during the World War I years, which may be spurious. The spatial pattern of the trend (Fig. 11, top right) indicates that the east–west pressure contrast over the Pacific Ocean has been decreasing since the turn of the century. There does not seem to be a consistent local relationship between the trend in SLP and that in SST. In some regions SLP is decreasing in time

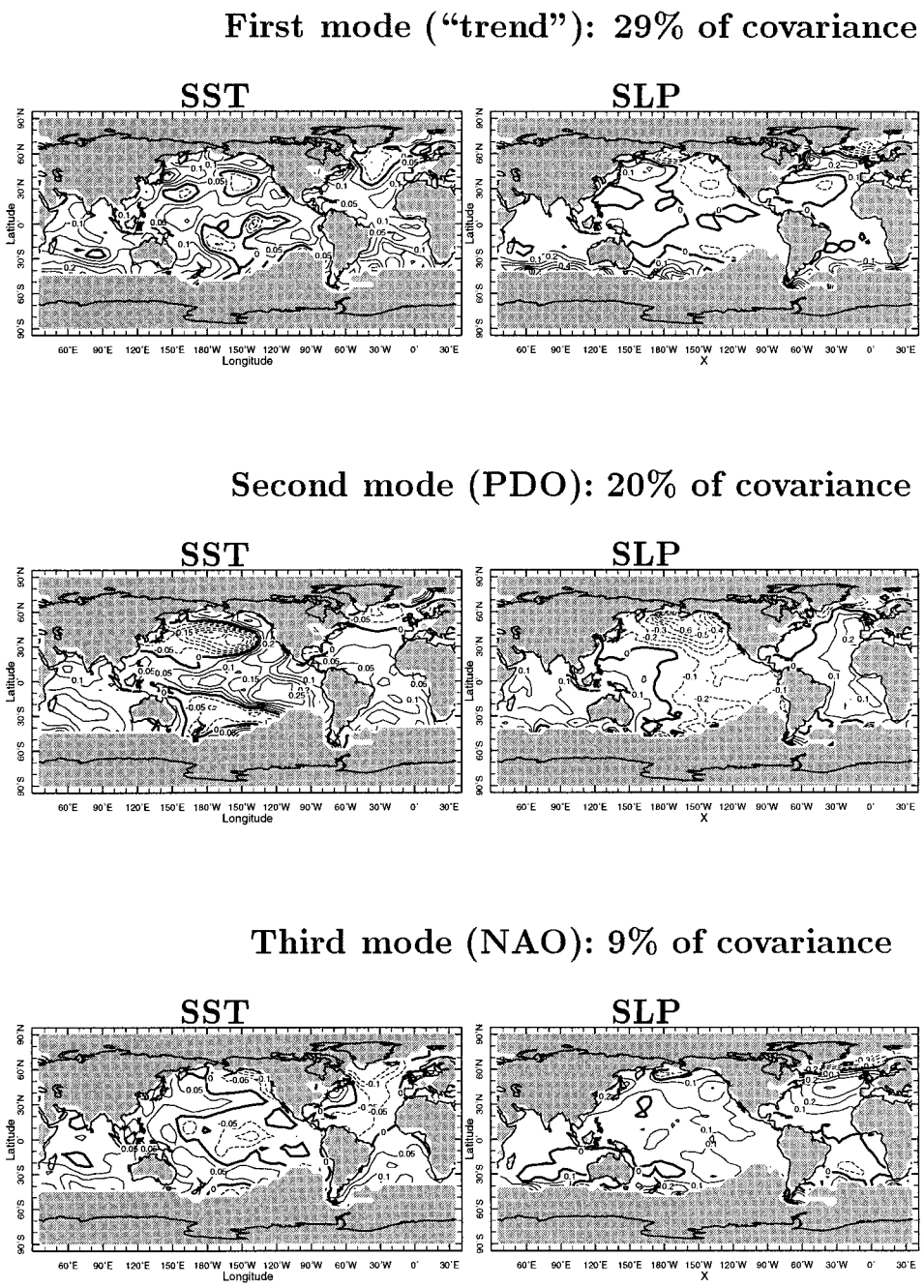

FIG. 11. Heterogenous regression patterns corresponding to the three leading SVD modes of SST and SLP covariance. SST patterns are in units of degrees Celsius per one standard deviation of SLP time series from Fig. 12; SLP patterns are in units of millibars per one standard deviation of SST time series from Fig. 12.

when SST is increasing, and in others the situation is reversed. Moreover, the pattern explains only 6% of the analysis area SLP variance and the heterogeneous correlation pattern (not shown) rarely displays values higher than 0.3, except over the southern edge of the analysis domain. Clearly further independent SLP data are needed to verify the authenticity of this pattern.

The second pattern of joint SLP and SST variability during the last century and a half is shown in the middle set of panels in Fig. 11. The corresponding time series are in the middle panel of Fig. 12. From its spatial structure and temporal characteristics the pattern can be easily recognized as that of the Pacific decadal oscillation (Zhang et al. 1997; Mantua et al. 1997). It rep-

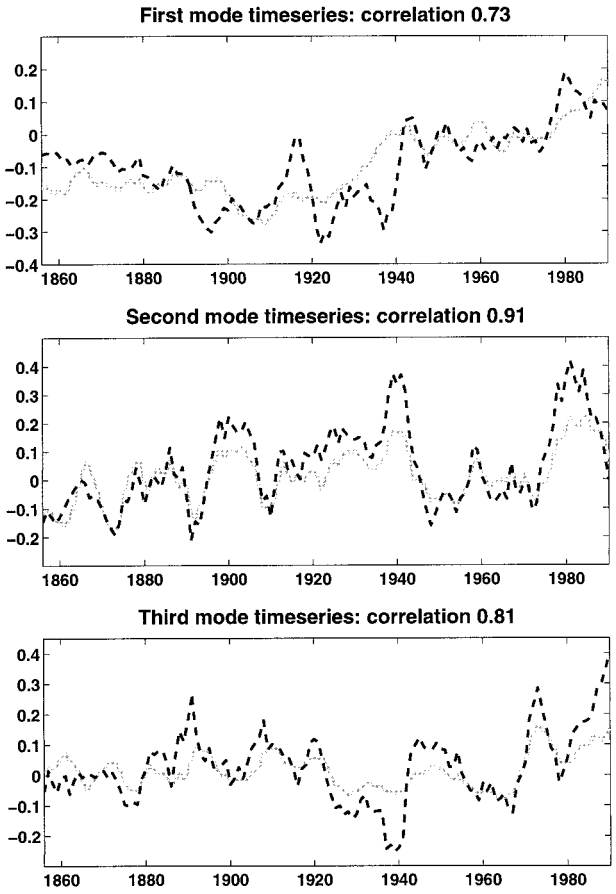

FIG. 12. Time series corresponding to the three leading SVD modes for SST (°C) (solid lines) and SLP (mb) (dashed lines).

resents the low-frequency manifestation of ENSO. The pattern entails an ''ENSO-like'' relationship between tropical and midlatitude Pacific SST, and between SST and SLP in the entire Pacific basin. South Atlantic and Indian Oceans SST vary in phase with those in the tropical Pacific and along the western North American seaboard. SLP in the Atlantic and the Indian Oceans varies in opposite polarity to that over the northern and eastern tropical Pacific, consistent with the signature of the Southern Oscillation. The time series of the SLP and SST patterns are correlated at a level of 0.91 and explain 20% of the total covariance between the two fields, and 15% and 18% of the analysis domain SST and SLP variance, respectively. The SST time series is significantly correlated (0.77) with the Niño-3 index, and the corresponding SLP series highly correlates (0.88) with the Trenberth and Hurrell (1994) North Pacific index.

The third pattern (bottom panels of Figs. 11 and 12) shows little SLP variability outside the North Atlantic basin. The latter consists of an out-of-phase fluctuation between the subpolar and subtropical Atlantic, resembling the NAO ''dipole'' (Hurrell 1995). The corresponding SST pattern is more global in extent, covering regions in both Atlantic and Pacific Ocean basins. In the Atlantic, SST north and south of the equator vary out of phase with each other in a manner akin to that displayed by the third SST eigenvector of Folland et al. (1986) (see also Parker and Folland 1991). There is.also some resemblance between the North Atlantic SST pattern and the interdecadal pattern of Atlantic SST variability described in Kushnir (1994; see also Kushnir and Held 1996). Note that the relationship between SST and SLP variability in the North Atlantic is somewhat different from that associated with interannual variability (Kushnir 1994; Kushnir and Held 1996). The temporal behavior of the SLP pattern is consistent with the low-frequency evolution of the NAO index shown in Hurrell (1995) and has a correlation of 0.78 with the latter. The relationship between Pacific SST and variability in the Atlantic basin is to some extent consistent with the Folland et al. (1986) analysis, but in addition reveals a link between the topical Pacific and decadal changes in the NAO. However, these features maybe spurious as the SST heterogeneous correlation pattern does not display large areas with correlation above 0.3, except in the North Atlantic and south Indian Ocean regions. As a result this climate variability pattern explains only 6% of the SST variance. The respective number for the SLP field is 9%. Overall this pattern explains 9% of the joint variability of the two fields and the time series correlate at a level of 0.81.

6. Discussion and summary

This first attempt at applying the reduced space OI analysis technique to marine SLP data shows some success. The open ocean SLP fields verify against the CDAS and UKMO analyses, products based on richer data sources; historical reconstructions of SLP indices are validated by land observations; the analysis error bars give reliable error estimates; large-scale long-term modes of variability are reasonable. However, aliasing of short-term SLP variability near land and on the southern edge of the analysis domain causes steep error increase in these areas. Comparison with other products that benefit from the land station data and principles of meteorological analysis suggests that those problems can be helped by bringing land data into the analysis. This will be our next step, to be carried out as soon as a coherent compilation of land station SLP records currently under development in the UKMO becomes available for our use. Incorporating land into such an analysis will make it almost global and will be beneficial in its own right. We also plan to test the use of the SLP fields of the CDAS reanalysis for the estimation of the reduced space patterns and energy distribution. However, the latter procedure will result in a dependence of the analysis on the CDAS assimilating model, a possible drawback in some regions. The difference between CDAS and COADS implied covariance structures, and the influence of the switching from one covariance estimate

to another on the results of optimal analysis, will have to be investigated. More elaborated versions of the analysis may involve seasonal variations of assumed covariance structure and make use of SST data via SST–SLP statistical connections.

The procedure of reestimating the signal covariance developed in this work achieves the consistency between the energy distribution in the solution with the a priori estimate of the reduced space signal covariance. However, it apparently overestimates the covariance in the truncated part of the spectrum. Inadequacy of the observational data sampling and the crudeness of our observational error model are the most probable culprits. While the possibilities of improving the former are limited, the latter can perhaps be refined in the future. The influence of this procedural caveat on the present product is not particularly detrimental: if anything, it results in the larger (more conservative) theoretical error estimates for the solution.

Among many things that could go wrong with this SLP analysis is the possible aliasing of diurnal and semidiurnal tides for the periods such as the beginning of the century (Barnett 1984) when the COADS data were sampled fewer than four times per day (Trenberth 1977). Effect of atmospheric tides can exceed 1 mb in the Tropics, but we see no evidence of the problem in our reconstruction of tropical indices. A possible explanation is that the tidal influence has a global structure of wavenumber 2 in the atmosphere (Trenberth 1991), which is not assigned much energy by our reduced space covariance structure, as the latter was estimated for the modern period of approximately four times per day data sampling. Also predominant data sampling in midlatitudes, where tidal influence is weaker, probably helps to filter out tropical aliasing.

A surprising finding of this work is that reconstruction of SLP indices based exclusively on ship observations can be competitive in quality with those based on land station records. However, all presently available datasets of marine observations start in the 1850s and have very poor data coverage over the first two decades, which limits the length of useful reconstructions for marine-based indices.

Acknowledgments. We are grateful to many colleagues for their interest to this work and generous help. Kevin Trenberth, David Parker, Phil Jones, Eugenia Kalnay, Rob Allan, Mike Evans, and Scott Woodruff read the manuscript and made many useful remarks and suggestions. Constructive remarks of two anonymous reviewers are particularly appreciated. Ed Cook discussed data availability and interpretation issues; Jim Simpson explained the subtleties of different definitions of SOI and helped with the data; Klaus Wolter, Dick Reynolds, Tom Smith, and Bob Livezey discussed the results. We are thankful to the U.K. Met. Office and Tracy Basnett for making their SLP analysis available to us. Benno Blumenthal's Ingrid software is responsible for all 2D plots in this work, and his Data Library system uses Senya Basin's CUF format for providing easy public access to the results of this work at http://ingrid.ldgo.columbia.edu/SOURCES/.KAPLAN/.RSA_COADS_SLP1.html. This work was supported by NOAA Grant UCSIO-10775411D/NA47GPO-188.

APPENDIX

Reestimation of the Signal Covariance

Kaplan et al. (1997) (hereafter K97) in their appendix B obtained equations

$$\mathbf{A}_p \overset{\text{def}}{=} \langle \boldsymbol{\alpha}^p \boldsymbol{\alpha}^{p\ \mathrm{T}} \rangle = \boldsymbol{\Lambda} + \mathcal{P}^p, \tag{A1}$$

$$\mathbf{A}_{\mathrm{OI}} \overset{\text{def}}{=} \langle \boldsymbol{\alpha}^{\mathrm{OI}} \boldsymbol{\alpha}^{\mathrm{OI}\ \mathrm{T}} \rangle = \boldsymbol{\Lambda}(\boldsymbol{\Lambda} + \mathcal{P}^p)^{-1}\boldsymbol{\Lambda}, \tag{A2}$$

which tie together covariances of the projection and reduced space OI solutions ($\boldsymbol{\alpha}^p$ and $\boldsymbol{\alpha}^{\mathrm{OI}}$, respectively), error covariance for the projection solution $\mathcal{P}^p$, and the covariance of the retained portion of the signal space, $\boldsymbol{\Lambda}$, presented for the basis defined by $\mathbf{E}$ [cf. Eq. (1)]. The projection solution $\boldsymbol{\alpha}^p$ consists of the best-fit coefficients for the predetermined set of patterns (the columns of $\mathbf{E}$) to the observed data. Covariance $\mathcal{P}^p$ is the theoretical estimate of the error in these coefficients.

The covariance $\boldsymbol{\Lambda}$ is the principal assumption in our computational procedure: it determines the distribution of energy over the basis of the reduced space. If the underlying assumptions of the method hold, the values of analyses covariances $\mathbf{A}_p$ and $\mathbf{A}_{\mathrm{OI}}$ obtained from the solution should be approximately equal to the theoretical values given by the respective right-hand sides of the equations (A1) and (A2). In particular, the covariance of the projection solution should exceed the assumed covariance of the ''true'' signal, while the latter should exceed the covariance of the OI. In K97 we tested this consistency by plotting the ratios of the diagonals of the analyses' covariances to the diagonal of $\boldsymbol{\Lambda}$. We expect the projection ratio to be larger than unity and the OI ratio to be smaller than unity. If no adjustment is made to the covariance found through our standard procedure, this consistency check fails for the present SLP analysis: both ratios are less than unity. This test did not hold for the unadjusted signal covariance in our SST analyses either, but a heuristic procedure was introduced that changed only the distribution of energy over the EOF modes and preserved the diagonality of $\boldsymbol{\Lambda}$. This approach implicitly assumed that the individual EOFs modes could be used as they are, without any rotation. Results of this procedure were quite satisfactory for the SST analysis (see Fig. 15 of K97) but failed for the present SLP analysis. Consequently, here we develop a more complete and less heuristic procedure based on Eqs. (A1) and (A2).

Inserting (A1) into (A2) to eliminate $\mathcal{P}^p$ yields

$$\mathbf{A}_p = \boldsymbol{\Lambda}\mathbf{A}_{\mathrm{OI}}^{-1}\boldsymbol{\Lambda}, \tag{A3}$$

in which $\mathbf{A}_p$ and $\mathbf{A}_{\mathrm{OI}}$ are the known estimates from the

projection and OI solutions, respectively, and $\mathbf{\Lambda}$ is being sought in the class of symmetric nonnegative definite matrices. An exact solution to the nonlinear matrix equation (A3) can be constructed in the following way. We define canonical decompositions of the symmetric positive matrices $\mathbf{A}_p$ and $\mathbf{A}_{\mathrm{OI}}$ by

$$\mathbf{A}_p = \mathbf{E}_p\mathbf{S}_p^2\mathbf{E}_p^{\mathrm{T}}, \qquad \mathbf{A}_{\mathrm{OI}} = \mathbf{E}_{\mathrm{OI}}\mathbf{S}_{\mathrm{OI}}^{-2}\mathbf{E}_{\mathrm{OI}}^{\mathrm{T}}, \tag{A4}$$

where $\mathbf{E}_p$ and $\mathbf{E}_{\mathrm{OI}}$ are orthogonal matrices, while $\mathbf{S}_p^2$ and $\mathbf{S}_{\mathrm{OI}}^2$ are positive diagonal matrices. Inserting Eq. (A4) into (A3) we obtain

$$\mathbf{E}_p\mathbf{S}_p^2\mathbf{E}_p^{\mathrm{T}} = \mathbf{\Lambda}\mathbf{E}_{\mathrm{OI}}\mathbf{S}_{\mathrm{OI}}^2\mathbf{E}_{\mathrm{OI}}^{\mathrm{T}}\mathbf{\Lambda}, \quad \text{or}$$

$$(\mathbf{E}_p\mathbf{S}_p)(\mathbf{E}_p\mathbf{S}_p)^{\mathrm{T}} = (\mathbf{\Lambda}\mathbf{E}_{\mathrm{OI}}\mathbf{S}_{\mathrm{OI}})(\mathbf{\Lambda}\mathbf{E}_{\mathrm{OI}}\mathbf{S}_{\mathrm{OI}})^{\mathrm{T}}.$$

The latter can be true if and only if there exists an orthogonal matrix $\mathbf{U}$ such that

$$\mathbf{E}_p\mathbf{S}_p\mathbf{U} = \mathbf{\Lambda}\mathbf{E}_{\mathrm{OI}}\mathbf{S}_{\mathrm{OI}},$$

and thus

$$\mathbf{\Lambda} = \mathbf{E}_p\mathbf{S}_p\mathbf{U}\mathbf{S}_{\mathrm{OI}}^{-1}\mathbf{E}_{\mathrm{OI}}^{\mathrm{T}}. \tag{A5}$$

Now our task is to choose $\mathbf{U}$ so that $\mathbf{\Lambda}$ defined by formula (A5) is symmetric and nonnegative definite. Symmetry means that

$$\begin{aligned}\mathbf{E}_p\mathbf{S}_p\mathbf{U}\mathbf{S}_{\mathrm{OI}}^{-1}\mathbf{E}_{\mathrm{OI}}^{\mathrm{T}} &= \mathbf{E}_{\mathrm{OI}}\mathbf{S}_{\mathrm{OI}}^{-1}\mathbf{U}^{\mathrm{T}}\mathbf{S}_p\mathbf{E}_p^{\mathrm{T}} \quad \text{or}\\ \mathbf{U}\mathbf{S}_{\mathrm{OI}}^{-1}\mathbf{E}_{\mathrm{OI}}^{\mathrm{T}}\mathbf{E}_p\mathbf{S}_p^{-1} &= \mathbf{S}_p^{-1}\mathbf{E}_P^{\mathrm{T}}\mathbf{E}_{\mathrm{OI}}\mathbf{S}_{\mathrm{OI}}^{-1}\mathbf{U}^{\mathrm{T}}\\ &= (\mathbf{U}\mathbf{S}_{\mathrm{OI}}^{-1}\mathbf{E}_{\mathrm{OI}}^{\mathrm{T}}\mathbf{E}_p\mathbf{S}_p^{-1})^{\mathrm{T}}.\end{aligned} \tag{A6}$$

We define the singular value decomposition of $\mathbf{S}_{\mathrm{OI}}^{-1}\mathbf{E}_{\mathrm{OI}}^{\mathrm{T}}\mathbf{E}_p\mathbf{S}_p^{-1}$ by

$$\mathbf{S}_{\mathrm{OI}}^{-1}\mathbf{E}_{\mathrm{OI}}^{\mathrm{T}}\mathbf{E}_p\mathbf{S}_p^{-1} = \mathbf{G}_1\mathbf{\Sigma}\mathbf{G}_2^{\mathrm{T}}; \tag{A7}$$

$\mathbf{G}_1$ and $\mathbf{G}_2$ being orthogonal matrices, and $\mathbf{\Sigma}$ being a diagonal matrix with nonnegative elements. Obviously, the choice

$$\mathbf{U} = \mathbf{G}_2\mathbf{G}_1^{\mathrm{T}}$$

makes

$$\mathbf{U}\mathbf{S}_{\mathrm{OI}}^{-1}\mathbf{E}_{\mathrm{OI}}^{\mathrm{T}}\mathbf{E}_p\mathbf{S}_p^{-1} = \mathbf{G}_2\mathbf{\Sigma}\mathbf{G}_2^{\mathrm{T}}$$

symmetric and thus satisfies Eq. (A6). As a result we have

$$\mathbf{\Lambda} = \mathbf{E}_p\mathbf{S}_p\mathbf{G}_2\mathbf{\Sigma}\mathbf{G}_2^{\mathrm{T}}\mathbf{S}_p\mathbf{E}_p^{\mathrm{T}}, \tag{A8}$$

which is obviously symmetric and nonnegative (as $\mathbf{\Sigma}$ is nonnegative). In order to compute the solution (A8) we perform matrix decompositions (A4) and (A7) using MATLAB software. All matrices involved in this computation has the order equal to the dimension L of a chosen reduced space ($L = 80$ in the present application).

The entire procedure of the analysis then performed in the following two-stage way. The covariance of the field is estimated; EOF patterns and eigenvalues are computed and used in projection and OI analyses without any adjustment. From the results of the analysis, $\mathbf{A}_p$ and $\mathbf{A}_{\mathrm{OI}}$ are estimated, as is the signal covariance $\mathbf{\Lambda}$, computed according to formula (A8). Canonical decomposition,

$$\mathbf{\Lambda} = \mathbf{F}\mathbf{\Lambda}_1\mathbf{F}^{\mathrm{T}},$$

shows that the EOF patterns found originally should be rotated by the operator $\mathbf{F}$ and the distribution of energy over these rotated (but still orthogonal!) patterns should be given by the elements of $\mathbf{\Lambda}_1$. EOFs not included into the reduced space are not being rotated, but their eigenvalues are modified according to the formula

$$\lambda_i^1 = \gamma\lambda_i + c, \qquad i = L + 1, \ldots, M,$$

where γ and c are constants that we defined from the two conditions: conservation of the total variance v of the spectrum

$$v = \mathrm{Tr}[\mathbf{\Lambda}_1] + \gamma(v - \mathrm{Tr}[\mathbf{\Lambda}]) + c(M - L),$$

and ''no-jump'' after the last reduced-space eigenvalue

$$\gamma\lambda_{L+1} + c = \lambda_L^1.$$

These conditions give the values of constants

$$\gamma = \frac{v - \mathrm{Tr}[\mathbf{\Lambda}_1] - \lambda_L^1(M - L)}{v - \mathrm{Tr}[\mathbf{\Lambda}] - \lambda_{L+1}(M - L)}, \qquad c = \lambda_L^1 - \gamma\lambda_{L+1}.$$

With this corrected estimate of covariance we rerun the analysis and check if Eqs. (A1) and (A2) hold for $\mathbf{A}_p$ and $\mathbf{A}_{\mathrm{OI}}$ estimated from its results (i.e., if the results of the analysis are consistent with our a priori assumption on the signal variance). If not, we could do another iteration. However, for this particular SLP applications the agreement was quite satisfactory.

To close the story, we examine why the heuristic algorithm of K97 failed for the SLP analysis, but not for the SST analysis of K98. For this we run our new covariance reestimation algorithm for the SST analysis of K98. The explanation is that the reduced-space EOF rotation matrix $\mathbf{F}$ for the SLP analysis has more offdiagonal structure than that for the SST analysis. Also the eigenvalues estimated by the present algorithm are much closer to those estimated by the K97 method for SST than for SLP.

As discussed in K97, a realistic estimate of the signal covariance is of crucial importance for obtaining realistic theoretical error estimates. When we repeat the experiment with the North Atlantic 1950–92 withheld area as in K97 and K98 we find that the theoretical error estimate in the middle of the North Atlantic withheld area reaches 0.8 mb, while when all the available data are used, the estimated error is about 0.3 mb [because this value includes large-scale error only (Fig. 1c), excluding the influence of truncation error (Fig. 1b), it is smaller than the North Atlantic error values in Fig. 2a and Table 3]. Consistent with these error estimates, the rms difference between the solutions with and without the data in the chosen area almost reaches 0.6 mb. This example is evidence that the analysis with the given

settings produces reliable conservative error estimates for the solution.

REFERENCES

Allan, R. J., J. A. Lindesay, and D. E. Parker, 1996: *El Niño Southern Oscillation and Climatic Variability.* CSIRO Publications, 405 pp.

Barnett, T. P., 1984: Long-term trends in surface temperature over the oceans. *Mon. Wea. Rev.,* **112,** 303–312.

Basnett, T. A., and D. E. Parker, 1997: Development of the global mean sea level pressure data set GMSLP2. Hadley Centre of the U.K. Meteorological Office for Climate Research, Tech. Note 79, 16 pp. [Available from the Hadley Centre for Climate Prediction and Research, Meteorological Office, London Road, Bracknell, Berkshire RS12 2SY, United Kingdom.]

Bottomley, M., C. K. Folland, J. Hsiung, R. E. Newell, and D. E. Parker, 1990: *Global Ocean Surface Temperature Atlas.* Her Majesty's Stationery Office, 20 pp.

Bretherton, C. S., C. Smith, and J. M. Wallace, 1992: An intercomparison of methods for finding coupled patterns in climate data. *J. Climate,* **5,** 541–560.

Cane, M. A., A. C. Clement, A. Kaplan, Y. Kushnir, R. Murtugudde, D. Pozdnyakov, R. Seager, and S. E. Zebiak, 1997: 20th century sea surface temperature trends. *Science,* **275,** 957–960.

Davis, R. E., 1976: Predictability of sea surface temperature and sea level pressure anomalies over the North Pacific Ocean. *J. Phys. Oceanogr.,* **6,** 249–266.

Folland, C. K., T. N. Palmer, and D. E. Parker, 1986: Sahel rainfall and worldwide sea temperatures 1901–85. *Nature,* **320,** 602–607.

Hurrell, J. W., 1995: Decadal trends in the North Atlantic Oscillation: Regional temperatures and precipitation. *Science,* **269,** 676–679.

——, and K. E. Trenberth, 1999: Global sea surface temperature analyses: Multiple problems and their implications for climate analysis, modeling, and reanalysis. *Bull. Amer. Meteor. Soc.,* **80,** 2661–2678.

Jones, P. D., T. Jónsson, and D. Wheeler, 1997: Extension to the North Atlantic Oscillation using early instrumental pressure observations from Gibraltar and South-West Iceland. *Int. J. Climatol.,* **17,** 1433–1450.

Kalnay, E., and Coauthors, 1996: The NCEP/NCAR 40-year reanalysis project. *Bull. Amer. Meteor. Soc.,* **77,** 437–471.

Kaplan, A., Y. Kushnir, M. A. Cane, and M. B. Blumenthal, 1997: Reduced space optimal analysis for historical datasets: 136 years of Atlantic sea surface temperatures. *J. Geophys. Res.,* **102,** 27 835–27 860.

——, M. A. Cane, Y. Kushnir, A. C. Clement, M. B. Blumenthal, and B. Rajagopalan, 1998: Analyses of global sea surface temperature 1856–1991. *J. Geophys. Res.,* **103,** 18 567–18 589.

Können, G. P., P. D. Jones, M. H. Kaltofen, and R. J. Allan, 1998: Pre-1866 extensions of the Southern Oscillation index using early Indonesian and Tahitian meteorological readings. *J. Climate,* **11,** 2325–2339.

Kushnir, Y., 1994: Interdecadal variations in North Atlantic sea surface temperature and associated atmospheric conditions. *J. Climate,* **7,** 141–157.

——, and I. M. Held, 1996: Equilibrium response to North Atlantic SST anomalies. *J. Climate,* **9,** 1208–1220.

Leith, C. E., 1973: The standard error of time-average estimates of climatic means. *J. Appl. Meteor.,* **12,** 1066–1069.

Mantua, N. J., S. R. Hare, Y. Zhang, J. M. Wallace, and R. C. Francis, 1997: A Pacific interdecadal climate oscillation with impacts on salmon production. *Bull. Amer. Meteor. Soc.,* **78,** 1069–1079.

Nicholls, N., G. V. Gruza, J. Jouzel, T. R. Karl, L. A. Ogallo, and D. E. Parker, 1996: Observed climate variability and change. *Climate Change 1995,* J. T. Houghton et al., Eds., Cambridge University Press, 133–192.

Parker, D. E., and C. K. Folland, 1991: Worldwide surface temperature trends since the mid-19th century. *Greenhouse-Gas-Induced Climatic Change: A Critical Appraisal of Simulations and Observations,* M. E. Schlesinger, Ed., Elsevier, 173–193.

——, P. D. Jones, C. K. Folland, and A. Bevan, 1994: Interdecadal changes of surface temperature since the late nineteenth century. *J. Geophys. Res.,* **99,** 14 373–14 399.

Ropelewski, C. F., and P. D. Jones, 1987: An extension of the Tahiti–Darwin Southern Oscillation index. *Mon. Wea. Rev.,* **115,** 2161–2165.

Shapiro, R., 1971: The use of linear filtering as a parameterization of atmospheric diffusion. *J. Atmos. Sci.,* **28,** 523–531.

Trenberth, K. E., 1977: Surface atmospheric tides in New Zealand. *N. Z. J. Sci.,* **20,** 339–356.

——, 1984: Signal versus noise in the Southern Oscillation. *Mon. Wea. Rev.,* **112,** 326–332.

——, 1991: Climate diagnostics from global analyses: Conservation of mass in ECMWF analyses. *J. Climate,* **4,** 707–722.

——, and D. A. Paolino, 1980: The Northern Hemisphere sea-level pressure data set: Trends, errors, and discontinuities. *Mon. Wea. Rev.,* **108,** 855–872.

——, and J. W. Hurrell, 1994: Decadal atmosphere–ocean variations in the Pacific. *Climate Dyn.,* **9,** 303–319.

——, and T. J. Hoar, 1996: The 1990–1995 El Niño–Southern Oscillation event: Longest on record. *Geophys. Res. Lett.,* **23,** 57–60.

——, J. R. Christy, and J. W. Hurrell, 1992: Monitoring global monthly mean surface temperatures. *J. Climate,* **5,** 1405–1423.

Woodruff, S. D., R. J. Slutz, R. L. Jenne, and P. M. Steurer, 1987: A comprehensive ocean–atmosphere data set. *Bull. Amer. Meteor. Soc.,* **68,** 1239–1250.

——, S. J. Lubker, K. Wolter, S. J. Worley, and J. D. Elms, 1993: Comprehensive Ocean–Atmosphere Data Set (COADS) Release 1a: 1980–92. *Earth Syst. Monit.,* **4,** 1–8.

——, H. F. Diaz, J. D. Elms, and S. J. Worley, 1998: COADS Release 2 data and metadata enhancements for improvements of marine surface flux fields. *Phys. Chem. Earth,* **23,** 517–526.

Zhang, Y., J. M. Wallace, and D. S. Battisti, 1997: ENSO-like interdecadal variability: 1900–93. *J. Climate,* **10,** 1004–1020.